



OPEN

# Room-Temperature Single-photon level Memory for Polarization States

SUBJECT AREAS:

QUANTUM  
INFORMATION

PHYSICS

Connor Kupchak, Thomas Mittiga, Bertus Jordaan, Mehdi Namazi, Christian Nölleke &amp; Eden Figueroa

Department of Physics and Astronomy, Stony Brook University, New York 11794-3800, USA.

Received  
24 September 2014Accepted  
3 December 2014Published  
7 January 2015Correspondence and  
requests for materials  
should be addressed to  
E.F. (eden.figueroa@  
stonybrook.edu)

An optical quantum memory is a stationary device that is capable of storing and recreating photonic qubits with a higher fidelity than any classical device. Thus far, these two requirements have been fulfilled for polarization qubits in systems based on cold atoms and cryogenically cooled crystals. Here, we report a room-temperature memory capable of storing arbitrary polarization qubits with a signal-to-background ratio higher than 1 and an average fidelity surpassing the classical benchmark for weak laser pulses containing 1.6 photons on average, without taking into account non-unitary operation. Our results demonstrate that a common vapor cell can reach the low background noise levels necessary for polarization qubit storage using single-photon level light, and propels atomic-vapor systems towards a level of functionality akin to other quantum information processing architectures.

A readily available, technologically simple, and inexpensive platform for optical quantum memories is the cornerstone of many future quantum technologies<sup>1–4</sup>. The practical implementation of such devices is fundamental to realizing deterministic logic gates for optical quantum computing<sup>5,6</sup>, and creating quantum repeater stations that overcome the current distance-limits of quantum key distribution<sup>7</sup>. A robust and truly scalable architecture may benefit from room-temperature, easy-to-operate quantum light-matter interfaces. Despite much progress<sup>8–13</sup>, the storage of polarization qubits in a room-temperature system has not yet been demonstrated<sup>14</sup>.

Room-temperature systems have shown much promise towards advanced optical technologies with progressions such as the miniaturization of vapor cells<sup>15</sup> and their integration into photonic structures for applications like light slow down<sup>16</sup>, four-wave mixing<sup>17</sup>, cross-phase modulation<sup>18</sup> and storage<sup>13</sup>. Furthermore, a warm vapor alleviates the need for laser trapping and cooling in vacuum or cooling to cryogenic temperatures.

The storage of light in atomic vapor can operate with high efficiency (87%)<sup>19</sup>, large spectral bandwidth (1.5 GHz)<sup>20</sup> and storage times on the order of milliseconds<sup>14</sup>. Vapor systems have proven their ability to preserve non-classical properties in the storage and retrieval of quantum light states<sup>14</sup>. In regard to qubits, polarization states were shown to be stored with high fidelity in experiments involving bright light pulses<sup>21,22</sup>. However, complete quantum memory operation [i.e. storage of polarization qubits] using warm atomic vapors has yet to be achieved<sup>14</sup> due to large control-field-related background photons constraining the *signal-to-background-ratio* (SBR) during retrieval.

Here we demonstrate a single-photon level, room-temperature implementation of an optical memory, by mapping arbitrary polarization states of light into and out of a warm rubidium vapor. The memory performance is tested with weak coherent pulses containing on average 1.6 photons. The average fidelity is measured to be  $71.5 \pm 1.6\%$ , with qubit coherence times on the order of 20  $\mu\text{s}$ . We also investigate the background noise and its relation to the memory fidelity.

To store a polarization qubit of the form  $|\psi_{in}\rangle = \cos\theta|H\rangle + e^{i\phi}\sin\theta|V\rangle$  (where  $|H\rangle$  and  $|V\rangle$  refer to horizontal and vertical polarization states and  $\theta$  and  $\phi$  correspond to the polar and azimuthal angles on the Poincaré sphere, respectively), we map the photonic polarization mode onto two spatially separated atomic ensembles concurrently under conditions of electromagnetically-induced transparency (EIT), in a single <sup>87</sup>Rb vapor cell at 62°C, containing Ne buffer gas (Figure 1a).

We employed two external-cavity diode lasers phase-locked at 6.8 GHz to resonantly couple a Lambda configuration composed of two hyperfine ground states sharing a common excited state. The probe field frequency is stabilized to the  $5S_{1/2}F = 1 \rightarrow 5P_{1/2}F' = 1$  transition at a wavelength of 795 nm (red detuning  $\Delta = 100$  MHz) while the control field interacts with the  $5S_{1/2}F = 2 \rightarrow 5P_{1/2}F' = 1$  transition.

The pulse shapes for both the probe and control fields are independently controlled with acousto-optical modulators. Two polarization beam displacers are used to create a dual-rail set-up allowing simultaneous light-

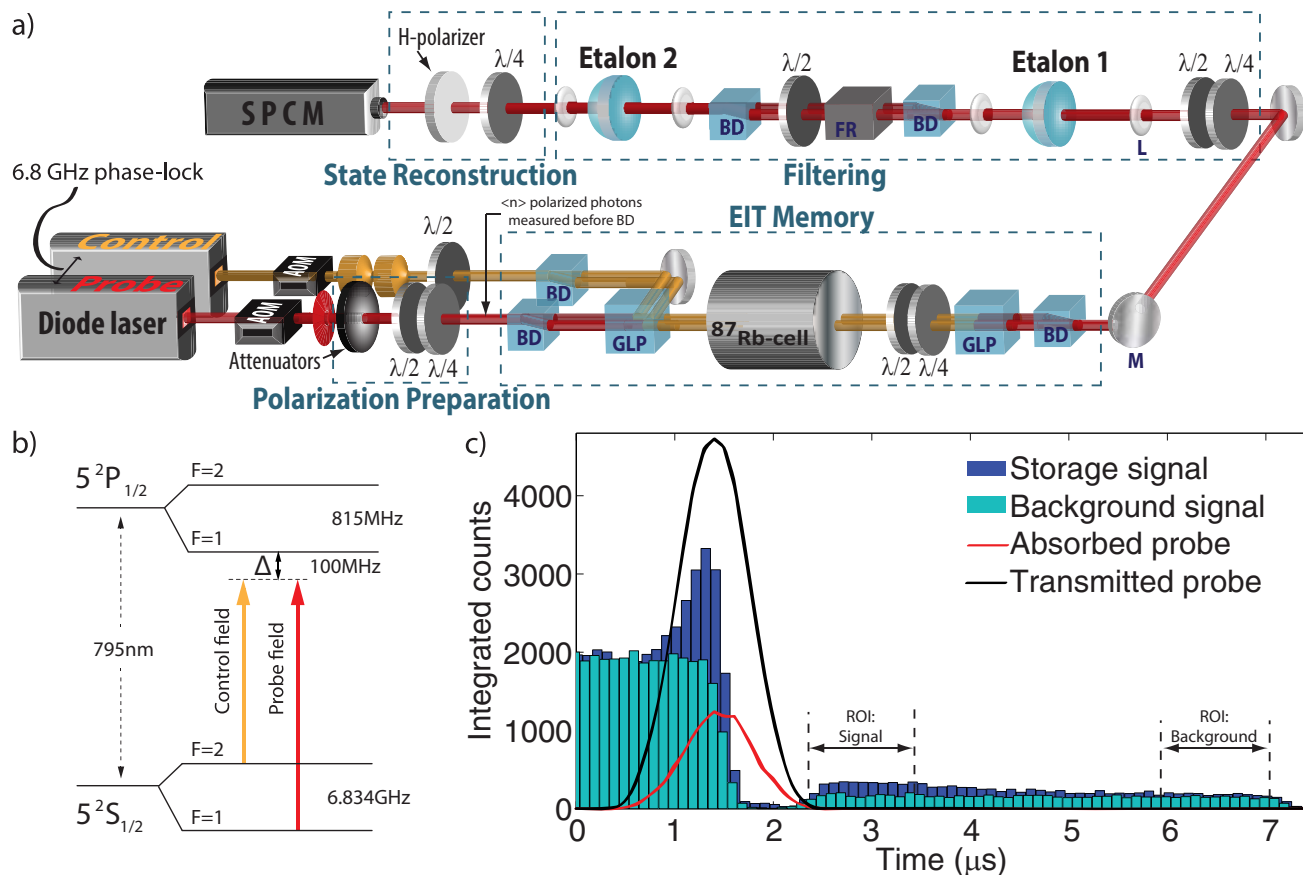


**Figure 1 | Experimental setup and photon-arrival histograms.** (a) Experimental setup for polarization qubit storage in rubidium vapor at the single-photon level, including the stages of control-filtering. AOM: Acusto-optical modulators; BD: Beam displacers; GLP: Glan-Laser-Polarizer; FR: Faraday rotator; SPCM: Single-Photon-Counting-Module; L: Lens; M: Mirror. Probe: red beam paths; control: yellow beam paths. (b) Atomic level scheme and EIT configuration. (c) Histograms of photon-arrival times, including the input pulse after transmission through the filtering stages (black line), input pulse after absorption in the cell (red line), storage experiment (blue bars) and background (light green bars). The region of interest (ROI) for the data analysis is also displayed.

storage in both rails. A set of polarization elements supply 42 dB of control field attenuation while maintaining 80% probe transmission. Furthermore, two monolithic, temperature-controlled etalon resonators provide a further 102 dB of control field extinction. Both etalons have a thickness of 7.5 mm, radius of curvature of 40.7 mm, free spectral range of 13.3 GHz, finesse of 310 and transmission linewidth of 43 MHz. Together they achieve a probe transmission of 16%. In between the etalons we have implemented a polarization insensitive Faraday isolator in order to suppress any back reflections off the etalon surfaces (transmission  $\sim 50\%$ ). Overall, our setup achieves 144 dB control field suppression while yielding a total 4.5% probe field transmission, hence exhibiting an effective, control/probe suppression ratio of 130 dB.

Storage experiments are performed with  $1 \mu\text{s}$  long probe pulses containing 1.6 photons for six different input polarizations  $|H\rangle$ ,  $|V\rangle$ ,  $|D\rangle = \frac{1}{\sqrt{2}}(|H\rangle + |V\rangle)$ ,  $|A\rangle = \frac{1}{\sqrt{2}}(|H\rangle - |V\rangle)$ ,  $|R\rangle = \frac{1}{\sqrt{2}}(|H\rangle + i|V\rangle)$ ,  $|L\rangle = \frac{1}{\sqrt{2}}(|H\rangle - i|V\rangle)$ , forming three mutually unbiased bases of the qubit Hilbert space. The resulting histograms of photon arrival times at the detector contain information regarding both the storage process and events associated to the control-field induced background (*storage histogram*, blue in Fig. 1c).

In order to determine the storage efficiency ( $\eta$ ) we integrate the number of counts over the region of interest (ROI) corresponding to the retrieved pulse (from 2.4 to 3.4  $\mu\text{s}$  in Fig. 1c) and subtract the number of counts from a signal-free region of the same histogram

(from 6 to 7  $\mu\text{s}$  in Fig. 1c). The efficiency is then calculated by comparing this difference in counts to the total counts in the transmitted probe through the filtering system without atomic interaction (black line in Fig. 1c). The signal to background ratio is obtained in a similar fashion using the counts integrated over the same ROI in the storage histogram (signal + background) and the number of counts over a signal-free region in the same histogram (background). Our SBR is then calculated as  $[(\text{signal} + \text{background}) - (\text{background})] / (\text{background})$  for each polarization input.

The polarization states retrieved from the EIT memory are evaluated using a polarimeter consisting of a quarter-wave plate and polarizer situated after the final filtering stage (see Fig. 1b). Rotating the quarter-wave plate causes oscillations in the intensity measured after the polarizer (within the previously defined ROI), from which we obtain the Stokes vectors ( $S = [S_0, S_1, S_2, S_3]$ , normalized by  $S_0$ ) through a fitting (see Fig. 2a–b)<sup>23</sup>.

The complete evaluation of the polarization fidelity is performed in four steps: First, we measure the Stokes parameters of our input probe polarization entering the first beam displacer. Second, we perform the same procedure for pulses that have propagated through the entire setup (cell included) and the filtering stages in the absence of EIT conditions (see Fig. 1c, red line). Third, we estimate and apply the unitary rotation to the original input states due to all optical elements by using a least squares fit method which fits them to the transmitted states without changing their lengths (see Fig. 2c).

The fidelity between the rotated inputs ( $S_{in}$ ) and the transmitted states was greater than 99% on average (green dots in Figure 3a). This

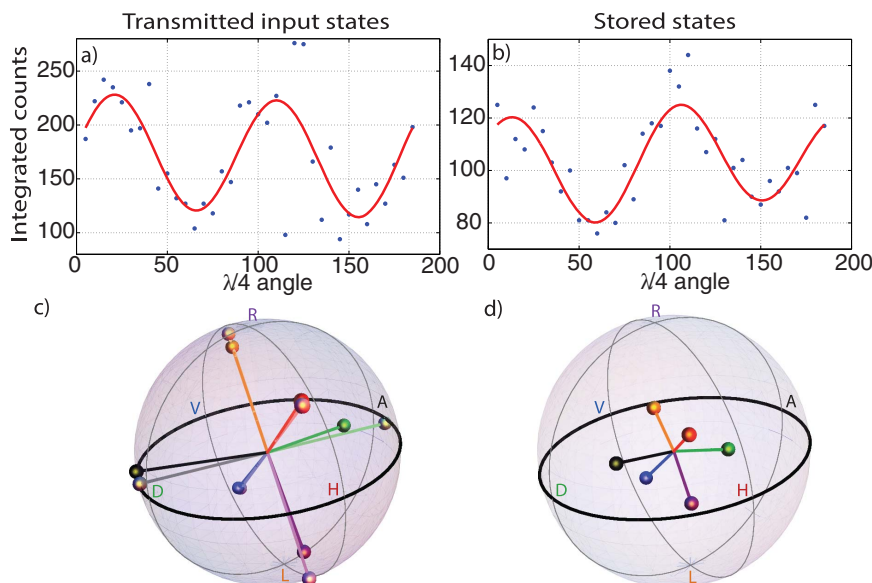


**Figure 2 | Polarization analysis.** Storage of polarization qubits at  $\langle n \rangle = 1.6$ . (a) Stokes reconstruction of  $|D\rangle$  transmitted input. (b) Stokes reconstruction of  $|D\rangle$  stored and retrieved output. The red line is the fitting used to estimate the Stokes vector. (c) Poincaré sphere of the transmitted input polarizations (bold colors) and Poincaré sphere of the rotated input polarizations (light colors). (d) Poincaré sphere of the stored and retrieved output polarizations.

step can alternatively be achieved in the system using linear optical elements. Lastly, we perform a polarization analysis of the retrieved pulses ( $S_{out}$ ) which are then compared directly to the rotated input states to obtain a fair estimation of fidelity with respect to the original input states. The fidelity is evaluated as  $F = \frac{1}{2} \left( 1 + S_{out} \cdot S_{in} + \sqrt{(1 - S_{out} \cdot S_{out})(1 - S_{in} \cdot S_{in})} \right)$ . We note this procedure is equivalent to utilizing the corresponding density matrices<sup>24</sup>.

In Figure 2d, the Poincaré sphere associated with the retrieved states clearly shows orthogonal but shortened vectors (as compared to the input) due to the influence of decoherence processes and the uncorrelated background counts. Table 1 summarizes the storage efficiency, SBR, and fidelity reconstruction for all the polarization inputs for  $\langle n \rangle = 1.6$  and shows an average fidelity of  $71.5 \pm 1.6\%$ . It is important to note that this fidelity value is dependent on the SBR and therefore reliant on the ROI being analyzed due to the dynamics of our memory system. The dependence of the fidelity associated with different ROIs can be explained by the temporal envelope of the retrieved signal being defined by two different time scales. The first is a coherently driven process (EIT retrieval at the beginning of the retrieved pulse) and a second incoherent contribution due to spontaneously emitted photons (latter part of retrieved pulse). Hence, by decreasing the ROI we post-select the coherent part of our retrieved signal. For instance, by reducing the ROI to 500 ns (2.5 to 3.1  $\mu\text{s}$ ) our average fidelity increases to  $74.3 \pm 1.6$  with an average SBR of  $1.61 \pm 0.14$ . This fidelity value is relevant since it is above the optimal classical fidelity for Poissonian distributed coherent states containing an average 1.6 photons and memory efficiencies of unity given by  $\langle F_{opt} \rangle = \sum_{n=1}^{\infty} F_{opt}(n) p_n / [1 - p_0] \approx 73.4\%$ , where  $p_n = e^{-\langle n \rangle} \langle n \rangle^n / n!$ . However, our measured fidelity is less than the classical threshold of 84.9% needed for more elaborate strategies that take into account the sub-unity efficiencies of our memory<sup>25,26</sup>. Nonetheless we will show that in our current physical conditions, our fidelity is more dependent on the SBR than the efficiency. Due to the small leakage of the control field, we also observe a weak vertical polarization of the mostly randomly polarized background noise which leads to higher fidelities for  $|V\rangle$  as shown in Table 1.

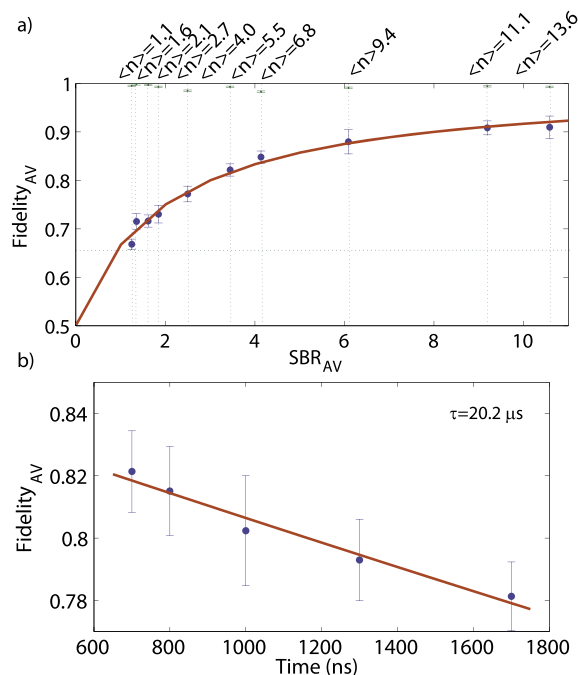


**Figure 3 | Analysis of the quantum memory.** (a) Scaling of the average fidelity of the qubit memory for varying signal-to-background ratio (transmitted states: green dots, retrieved states: blue dots). Shown in black are the average input photon numbers and the corresponding average signal-to background ratio. The red line shows the results of a theoretical model considering a dual-rail optical quantum memory, assuming each ensemble to be a Poissonian source of uncorrelated signal and background photons. (b) Coherence time measurement for  $\langle n \rangle = 6$  (blue dots) and lifetime fitting (red line). The error bars correspond to the standard error of the mean of the individual state fidelities and outweighs the errors associated with the individual state fidelity measurements.



Table 1 | Storage of polarization states in ROI

Input	H	V	D	A	R	L	Average
SBR	1.68	1.1	1.27	1.15	1.53	1.38	1.35 ± .09
Fidelity (%)	71.3	79	69.2	71.4	70.2	67.6	71.5 ± 1.6
Efficiency ( $\eta$ ) (%)	7.9	5.3	4.6	3.8	5.6	5.9	5.5 ± .6

To quantify the influence of the background on the fidelity of the qubit memory, we have performed a series of polarization measurements (using the ROI as before), where we modify the SBR by increasing the input photon number (see Figure 3a). We can see that an average fidelity of  $\sim 85\%$  (the classical threshold necessary when considering our memory efficiencies) can be achieved with a SBR of  $\sim 4.0$ , which is a four-fold increase over our current experimental implementation at the single photon level. The maximum achievable fidelity is ultimately limited by the technical imperfections of the setup and the decoherence of the hyperfine ground state superposition. The scaling of SBR can be understood with a theoretical model considering a dual-rail optical quantum memory based on two atomic ensembles, with each ensemble assumed to be a Poissonian source of uncorrelated signal and background photons.

We assume that each of the ensembles stores one of the two polarization components with efficiency  $\eta$  before recombination and read out. The probability of producing  $n$  signal photons and  $m$  background photons (for both ensembles) is  $P'_s(n) = \frac{(\eta p)^n}{n!} e^{-\eta p}$  and  $P'_{bg}(m) = \frac{q^m}{m!} e^{-q}$  respectively. Here  $p$  is the average number of input photons, and  $q$  is the average number of background photons. Note that two ensembles emitting Poissonian noise with mean photon number  $q/2$  into the same spatial mode behave as one noise source with mean photon number  $q$ .

In the instance of  $n$  signal and  $m$  background photons being produced, the probability of detecting a signal photon is simply  $\frac{n}{n+m}$ , and of detecting a background photon is  $\frac{m}{n+m}$  for non photon-number resolving detectors. Then, in general, the probabilities of detecting up to order  $N$  signal  $P_s(\eta, p, q, N)$  and background  $P_{bg}(\eta, p, q, N)$  photons are

$$P_s(\eta, p, q, N) = \sum_{n=0}^N \sum_{m=0}^N P'_s(n) P'_{bg}(m) \frac{n}{n+m} \quad (1)$$

$$P_{bg}(\eta, p, q, N) = \sum_{n=0}^N \sum_{m=0}^N P'_s(n) P'_{bg}(m) \frac{m}{n+m}, \quad (2)$$

and the fidelity is

$$F = \frac{P_s(\eta, p, N) + \frac{1}{2} P_{bg}(\eta, p, q, N)}{P_s(\eta, p, q, N) + P_{bg}(\eta, p, q, N)}. \quad (3)$$

The theoretical estimation for the fidelity scaling (solid red line in Fig. 3a) has been calculated using independently measured parameters  $\eta = 0.055$  and  $q = 0.005$  (see Figs. 4a–b).

Additionally, we have also measured the coherence time of the qubit storage. Due to the dependence of the memory fidelity on the SBR we would expect the fidelity to decay exponentially with the efficiency. Figure 3b shows the decay time of the memory for

the case  $\langle n \rangle = 6$ , showing a  $1/e$  time of  $20.2 \pm 0.2 \mu\text{s}$  which is about the same order of magnitude as the duration of our input pulses.

Furthermore, we experimentally characterize the background noise. To do so we integrate the number of counts in the ROI of histograms corresponding to measurements of only the background (cell present, control field only, green dots in Fig. 4a) and only the technical background (control field only, no cell, red dots in Fig. 4a) and divide by the number of experimental runs. This provides the number of background counts per retrieved pulse. We repeat this procedure for several values of the control field power.

We can see that the total background is composed of photons from both leakage of the control field (technical background) and those generated by atomic processes such as spontaneous Raman scattering and four-wave mixing<sup>27,28</sup>. The purple dots in Fig. 4a show the resultant of the technical counts subtracted from the background and the red line is a fitting of a function  $\propto \sqrt{\text{POWER}_{\Omega_c}}$  (or the square root of the control field power), where  $\Omega_c$  is the Rabi frequency of the control field. The nature of the square root dependence of our noise due from atomic interaction is the subject of current investigations.

Lastly, we analyze the behaviour of the storage efficiency in the ROI ( $\eta$ , blue dots in Fig. 4b) and SBR (using the same ROI, green points in Fig. 4b) as a function of the control field power. We can see that the efficiency has a substantially different scaling than the SBR and that their maxima do not match. We notice that while our setup is capable of maximum storage efficiencies of  $\eta_{max} \sim 16\%$  (over a larger ROI), the ideal signal to background value for quantum memory functionality corresponds to suboptimal storage efficiencies.

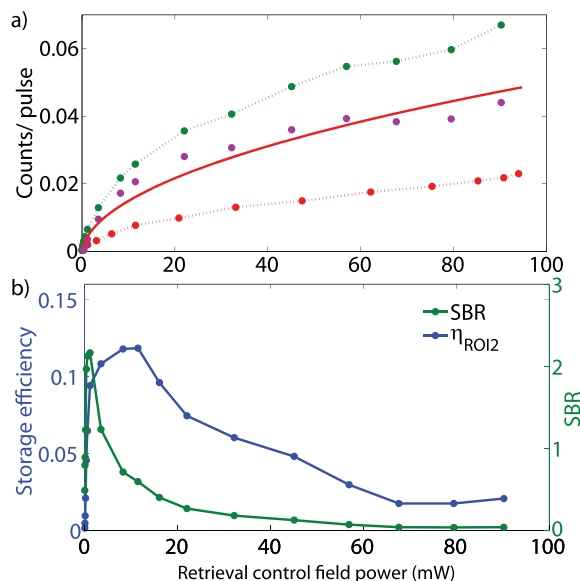


**Figure 4 | Background noise characterization.** (a) Counts in ROI per retrieved pulse for background (green dots) and technical background (control field only, no cell, red dots) with increasing control field power. The purple dots show the background counts with the technical counts subtracted and the red line is a fitting of a function  $\propto \sqrt{\text{POWER}_{\Omega_c}}$ . (b) Storage efficiency in the ROI (blue dots) and signal to background (green dots) as a function of control field power.



In summary, we have presented the first, to our knowledge, room-temperature single-photon level optical memory system capable of storing arbitrary polarization states. We have demonstrated an average fidelity of  $71.5 \pm 1.6\%$  ( $74.3 \pm 1.6\%$  with reduced ROIs) and storage lifetimes of  $\sim 20 \mu\text{s}$ . Our memory fidelity is strongly related on the SBR and can surpass certain classical benchmarks (not including storage efficiency) depending on the ROI analyzed. We have also investigated the influence of the background in the fidelity of the qubit memory and provided a model explaining the scaling of fidelity with signal-to-background ratio. These measurements demonstrate that a four-fold decrease in background is still necessary for our current implementation to operate with fidelities above the classical threshold ( $>85\%$ ) at our current efficiencies. This could be achieved by using an additional re-pumper scheme<sup>29</sup> or by modifying the one-photon detuning of the laser system. Longer coherence times can be achieved by adding paraffin coating to our current cells<sup>30</sup>. We believe that the present system has the potential to be implemented on a grand scale and thus paves the way for the creation of novel quantum repeaters and networks based on truly scalable architectures.

- Kimble, H. J. The quantum internet. *Nature* **453**, 1023 (2008).
- Lvovsky, A. I., Sanders, B. C. & Tittel, W. Optical quantum memory. *Nature Photonics* **3**, 706 (2009).
- Bussieres, F. *et al.* Prospective applications of optical quantum memories. *J. Mod. Opt.* **60**, 1519 (2013).
- Northup, T. E. & Blatt, R. Quantum information transfer using photons. *Nature Photonics* **8**, 356 (2014).
- Xu, X. F., Bao, X. H. & Pan, J. W. Demonstration of active feedforward one-way quantum computing with photon-matter hyperentanglement. *Phys. Rev. A* **86**, 050304 (2012).
- Monroe, C. *et al.* Large-scale modular quantum-computer architecture with atomic memory and photonic interconnects. *Phys. Rev. A* **89**, 022317 (2014).
- Duan, L. M., Lukin, M. D., Cirac, J. I. & Zoller, P. Long-distance quantum communication with atomic ensembles and linear optics. *Nature* **414**, 413 (2001).
- Maurer, P. C. *et al.* Room-Temperature Quantum Bit Memory Exceeding One Second. *Science* **336**, 1283 (2012).
- Saeedi, K. *et al.* Room-Temperature Quantum Bit Storage Exceeding 39 Minutes Using Ionized Donors in Silicon-28. *Science* **342**, 830 (2013).
- Eisaman, M. D. *et al.* Electromagnetically induced transparency with tunable single-photon pulses. *Nature* **438**, 837 (2005).
- Reim, K. F. *et al.* Single-Photon-Level Quantum Memory at Room Temperature. *Phys. Rev. Lett.* **107**, 053603 (2011).
- Hosseini, M. *et al.* Unconditional room-temperature quantum memory. *Nature Physics* **7**, 794 (2011).
- Sprague, M. R. *et al.* Broadband single-photon-level memory in a hollow-core photonic crystal fibre. *Nature Photonics* **8**, 287 (2014).
- Novikova, I., Walsworth, R. L. & Xiao, Y. Electromagnetically induced transparency-based slow and stored light in warm atoms. *Laser and Photonics Reviews* **6**, 333–353 (2012).
- Balukhsian, T. *et al.* Fabrication method for microscopic vapor cells for alkali atoms. *Opt. Lett.* **35**, 1950 (2010).
- Ghosh, G. *et al.* Low-Light-Level Optical Interactions with Rubidium Vapor in a Photonic Band-Gap Fiber. *Phys. Rev. Lett.* **97**, 023603 (2006).
- Londero, P. *et al.* Ultralow-Power Four-Wave Mixing with Rb in a Hollow-Core Photonic Band-Gap Fiber. *Phys. Rev. Lett.* **103**, 043602 (2009).
- Venkataraman, V., Saha, K. & Gaeta, A. L. Phase modulation at the few-photon level for weak-nonlinearity-based quantum computing. *Nature Photonics* **7**, 138 (2013).
- Hosseini, M. *et al.* High efficiency coherent optical memory with warm rubidium vapour. *Nature Communications* **2**, 174 (2011).
- Reim, K. F. *et al.* Towards high-speed optical quantum memories. *Nature Photonics* **4**, 218 (2010).
- Cho, Y.-W. & Kim, Y.-H. Atomic vapor quantum memory for a photonic polarization qubit. *Opt. Exp.* **18**, 25786 (2010).
- England, D. G. *et al.* High-fidelity polarization storage in a gigahertz bandwidth quantum memory. *J. Phys. B: At. Mol. Opt. Phys.* **45**, 124008 (2012).
- Berry, H. G., Gabrielse, G. & Livingston, A. E. Measurement of the Stokes parameters of light. *App. Opt.* **16**, 3200 (1977).
- Altepeter, J. B., Jeffrey, E. R. & Kwiat, P. G. Photonic State Tomography. *Adv. in Atom. Mol. and Opt. Phys.* **52**, 105–159 (2005).
- Specht, H. P. *et al.* A single-atom quantum memory. *Nature* **473**, 190 (2011).
- Gündoğan, M. *et al.* Quantum Storage of a Photonic Polarization Qubit in a Solid. *Phys. Rev. Lett.* **108**, 190504 (2012).
- Phillips, N. B., Gorshkov, A. V. & Novikova, I. Light storage in an optically thick atomic ensemble under conditions of electromagnetically induced transparency resonances in Rb vapor. *Phys. Rev. A* **83**, 063823 (2011).
- Lauk, N., O'Brien, C. & Fleischhauer, M. Fidelity of photon propagation in electromagnetically induced transparency in the presence of four-wave mixing. *Phys. Rev. A* **88**, 013823 (2013).
- Jiang, W., Chen, Q. F., Zhang, Y. S. & Guo, G.-C. Optical pumping-assisted electromagnetically induced transparency. *Phys. Rev. A* **73**, 053804 (2006).
- Balabas, M. V., Karaulanov, T., Ledbetter, M. P. & Budker, D. Polarized Alkali-Metal Vapor with Minute-Long Transverse Spin-Relaxation Time. *Phys. Rev. Lett.* **105**, 070801 (2010).

## Acknowledgments

We thank A. I. Lvovsky and A. J. MacRae for sharing their etalon design. This work was supported by the US-Navy Office of Naval Research, grant number N00141410801 (instrumentation) and the National Science Foundation, grant number PHY-1404398 (personnel and materials). The authors kindly thank G. Rempe, S. Ritter, A. Neuzner, J. Schupp and A. Reiserer for useful discussions. C. K. acknowledges financial support from the Natural Sciences and Engineering Research Council of Canada.

## Author contributions

C.K., T.M., B.J., M.N., C.N. and E.F. all contributed to the implementation and modelling of the experiment, the interpretation of the results and the writing of the manuscript.

## Additional information

**Competing financial interests:** The authors declare no competing financial interests.

**How to cite this article:** Kupchak, C. *et al.* Room-Temperature Single-photon level Memory for Polarization States. *Sci. Rep.* **5**, 7658; DOI:10.1038/srep07658 (2015).



This work is licensed under a Creative Commons Attribution-NonCommercial-NoDerivs 4.0 International License. The images or other third party material in this article are included in the article's Creative Commons license, unless indicated otherwise in the credit line; if the material is not included under the Creative Commons license, users will need to obtain permission from the license holder in order to reproduce the material. To view a copy of this license, visit <http://creativecommons.org/licenses/by-nc-nd/4.0/>